

Higher-radix Quantum Photonic Informatics and Implementation Issues in Integrated Circuits

MITCHELL A. THORNTON* AND DUNCAN L. MACFARLANE

Darwin Deason Institute for Cyber Security, Southern Methodist University, USA

Accepted: October 20, 2024.

Advances in fabrication methods and components are enabling practical implementations of Quantum Photonic Integrated Circuits (QPIC) analogous to the 1970's era for electronic integrated circuits (IC). As was the case more than 50 years ago in electronics, designers are faced with a choice regarding the physical quantities to use for encoding discrete information in a QPIC. Among the alternatives, models for information representation include binary and higher-radix, approaches. In the spirit of seminal writings from Professor K.C. Smith regarding the choice of radices for electronic switching circuits, we survey higher-dimensional QPIC implementations. We address various means for photonic representation of information and the tradeoffs that result in view of the current state of the art in available QPIC components and manufacturing capabilities. These alternatives are intended to inform the multiple-valued logic community of QPIC design choices and to draw an analogy to Professor Smith's earlier work in higher-radix electronic IC.

Keywords: Higher-radix, MVL, quantum photonics, QPIC

1 INTRODUCTION

One of Professor K.C. Smith's seminal papers entitled "Circuits for Multiple Valued Logic – A Tutorial and Appreciation" authored in 1976 [1] began with this sentence:

"It has been stated often in the past that practical acceptance of multi-valued logic awaits the development of suitable electronic means for fabricating a sufficiently powerful and general-purpose logic."

* Contact author: E-mail: mitch@lyle.smu.edu

Since Professor Smith's 1976 quotation and the time of writing of this paper, many engineers, scientists, mathematicians and others have investigated what is now known as "multiple-valued logic*," with a significant percentage of these investigations motivated by the pursuit of exploiting higher-radix systems to achieve classical electronic circuit solutions that offer advantages in comparison to binary switching implementations. While limited success has been achieved in some applications such as four-valued memory circuits and three-valued arithmetic circuits, it has generally been the case that the advantages gained from electronic integrated circuit scaling has outweighed any potential advantage that multiple-valued electronic circuitry could provide. One reason for this situation is that voltage-mode CMOS-based circuitry has emerged as the predominant form, likely due to its desirable power dissipation properties. The use of voltage-mode circuits in conjunction with increased component density due to fabrication advances causes the power rail voltages to correspondingly decrease and hence the noise margins around each represented logic value must also decrease. Therefore, increasing the number of logic values and their accompanying noise margin ranges while also compensating for ever-decreasing overall rail-to-rail voltage ranges becomes impractical as was aptly stated by Professor Smith in his tutorial article [2]. This leads to a design choice wherein the first choice is to use fewer and larger transistors to practically implement higher-radix circuitry versus the second choice of using more and smaller transistors to implement binary-radix circuitry. In considering the predominant design choice made for electronic switching circuits over the past 50 years as empirical evidence, it is this latter case of binary-radix switching circuitry that has generally predominated indicating that the binary-radix usually provides the better engineering solution.

Here, we respectfully propose that one response to Professor Smith's visionary quote above is that perhaps the "practical acceptance of multivalued logic" may not necessarily result from "suitable electronics," in part due to the reasons provided above, rather it may be "suitable quantum photonics" that ushers in an era of "practical acceptance of multivalued logic." This proposition is based upon the observation that the quantum characteristics of a photon offer the choice of several different measurable characteristics that naturally lend themselves to the realization of systems that are conveniently modeled with a multiple-valued logic framework as compared to the rather limited set of quantities available in classical electronic circuits.

In another of Professor Smith's early papers entitled "The Prospects for Multivalued Logic: A Technology and Applications View" [3], he identifies

* The term "multiple-valued logic" is commonly used, although the lesser-used term "many-valued logic" may be a more literal and precise description of this topic.

three measurable characteristics of electronic circuitry that could potentially be used to represent multiple-valued logic variables; namely ‘charge,’ ‘voltage’ and ‘current.’ In a similar manner, it is the objective of this paper to likewise present and discuss the various measurable characteristics of quantum photonic circuits that may serve as encodings of a multiple-valued logic framework. We note that in the contemporary literature on this topic, the more common adjective for describing discrete variable non-binary quantum photonic systems is “higher-dimensioned” rather than “multiple-valued,” and we shall henceforth use that term for the purposes of adhering to common convention, although the concepts are very similar.

In quantum photonic circuits, the measurable quantities, or “observables,” suitable for encoding multiple logic values in a higher-dimensioned system arise from forms of the several conjugate uncertainty variable pairs such as position and momentum. For single photon systems, these measurable quantities include the location of a photon, its frequency, temporal angular momentum or polarization and spatial angular momentum. For systems comprising a small number of photons, a measurable characteristic is the number of photons within a time or space interval, known as the “number” or “Fock state,” as well as their coherent phase, polarization and frequency values.

At the present time, many of the quantum photonic variables that were previously shown to be of use in table-top circuit implementations are now emerging for use in integrated circuit realizations due to optical components being available and configured in the form of “quantum photonic integrated circuits” (QPIC). New fabrication materials and processes as well as new miniaturized components are emerging and fabrication foundries are beginning to offer cell libraries and “software design kits” (SDK) to support fab-less design of QPICs [4, 5]. QPICs offer an exciting alternative to classical electronic “application specific integrated circuits” (ASIC) in terms of information processing due to their potential to exploit the “quantum advantage” which is the ability to process information much faster than would be possible through using an ASIC [6].

In the spirit of Professor Smith’s interest in realizing electronic multiple-valued logic circuits, we likewise discuss some of the measurable quantities of photons that are suitable for encoding and processing information within QPIC realizations.

2 QUANTUM PHOTONIC BACKGROUND

A photon is the smallest possible unit, or quantum, of electromagnetic (EM) field energy often colloquially described as a “particle of light” although it has a zero-valued rest mass. Photons have the same properties as classical

EM waves such as frequency, wavelength, polarization and others. Due to the concept of “matter waves” [7] photons also have properties such as position and momentum that are more commonly associated with particles comprising mass. Although photons are usually considered in terms of light, the visible portion of EM energy, photon quanta exist across the entire EM spectrum. Furthermore, photons are always moving[†] with a constant speed c in a vacuum.

The concept of light particles or photons is generally attributed to Einstein’s famous explanation of the photoelectric effect in his 1905 paper [8] where he generalized Planck’s blackbody radiation studies five years earlier although the concept was also proposed by earlier philosophers and physicists including Newton. Prior to Einstein’s seminal work, the predominant theory of light was considered classically as continuous traveling waves that adhere to Maxwell’s equations or the “classical field theory” of EM. A few years following the initial emergence of the theory of quantum mechanics (QM), Dirac is credited with “quantum field theory” (QFT) resulting from the so-called “second factorization” that provided a unifying framework for classical field theory, special relativity and quantum mechanics. After the theoretical developments of QM and QFT in the early part of the 20th century, a flurry of theoretical and experimental results followed. Of particular interest in this paper, are the results that taught us how photons interact with other particles at the quantum level and the applications of such interactions in terms of information representation and processing, or quantum informatics [9]. These results have led to the ability to design and fabricate engineering artifacts, including QPICs, based upon the quantum properties of photons.

Engineering artifacts are produced through innovation and invention motivated by societal needs. This creative process uses scientific discoveries as an underlying basis to enable new systems and processes to be devised with a goal of benefiting humanity. A QPIC is an example of such an engineering artifact that is enabled, in part, by QM/QFT theory.

“Quantum Informatics” (QI) is an engineering field wherein the sensing or acquisition, transfer or communication, and transformation or processing of information is accomplished through the application of QM/QFT in the design of an artifact such as a QPIC. This leads to the fundamental concept of using quantum theory to encode or represent information. Fortunately, the quantum nature of the photon can be used in a variety of different ways to encode information [10, 11].

A primary goal of this paper is to describe several of the different ways that information can be represented or encoded using photons. Another goal

[†] “Always moving” is a typical state although photons can be confined to small volumes such as within a resonant cavity or portions of a waveguide where differences in the index of refraction of the two materials whose interface forms a boundary, confine their location due to total internal reflection.

of this paper is underscore the analogy among different choices for photonic information representation as described here and those of electronic information representation as considered in the early papers of K.C. Smith that were mentioned in the previous section. While many of the ideas proposed for multiple-valued information representation in electronics did not find widespread usage in electronic information systems, we hypothesize that this may not be the case for quantum photonic information artifacts such as a QPIC or others within the field of QI.

2.1 Salient Points of Quantum Photonic Informatics

While a comprehensive review of quantum photonic theory and its application in QI is beyond the scope of this paper, many excellent textbooks and other works are available for the interested reader including [12–14]. Nevertheless, a summary of some of the key points of quantum photonics are given with the hope that this paper will be accessible to non-practitioners of quantum photonics in QI, but whom have a familiarity with multiple-valued logic and its application in information representation. Additionally, we introduce some of the notation that is commonly used in the quantum photonics community so that concepts of quantum photonic information representation can be provided in a precise manner.

2.2 Oscillators, the Hamiltonian and State Vectors

Although basic QM theory can be described in a variety of different ways, a common method is consideration of the quantum harmonic oscillator as a starting point [15]. At the birth of QM, Planck modeled atoms that absorb and emit EM radiation as an oscillator. However, the key difference Planck introduced in his oscillator model of the atom is that the total energy of an atom can only exist at discrete quantities, the process of quantization, thus causing his model to take the form of a “quantum” harmonic oscillator. In comparing the quantum harmonic oscillator to a continuous harmonic oscillator; for example, a mechanical clock’s pendulum in a constant gravitational field but without the presence of energy loss due to practical factors like bearing friction or air resistance, then the total energy of the idealized pendulum, E_{pen} , would be the sum of its kinetic energy, T_{pen} , due to its momentum and its potential energy, V_{pen} , due to the gravitational force that pulls it to its vertical position $E_{\text{pen}} = T_{\text{pen}} + V_{\text{pen}}$. In this clock pendulum example, we assume that an amount of energy is initially transferred to the pendulum at time, t_0 , due to the work imparted by an external force, \mathbf{f}_x , that pulls the pendulum to one side and moves it to a vertical distance of, z_0 , relative to the x -axis, to initiate its oscillatory motion as shown in Figure 1a. After the initial transfer of energy into the idealized clock pendulum occurs at time t_0 due to the work performed by the initial force, \mathbf{f}_x , at time, t_0 , the pendulum begins swinging

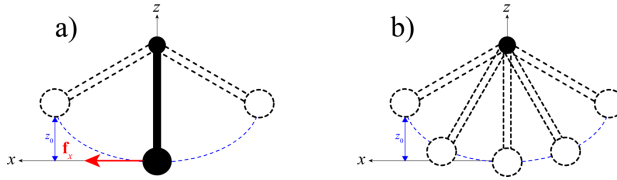


FIGURE 1

Idealized Clock Pendulum as Simple Harmonic Oscillator; a) Initial Energy Transfer into the Pendulum by Performing Work; b) Discretized Model of the Ideal Pendulum with $N = 5$ Finite Energy States.

back and forth in a continuous motion, oscillating about the vertical axis, z , and moving along the path indicated by the blue dashed arc in Figure 1.

If a quantization were to be applied to the clock pendulum, then an analogy to the non-relativistic quantum harmonic model would emerge that indicates the position of the pendulum could only be allowed to occupy certain discrete initial positions in space and it would no longer swing in an arbitrary continuous arc back and forth with respect to the vertical. Rather, to model discrete changes in total energy, E_{pen} , it would instantaneously move from one discrete position to another as indicated by the dashed outlines of the pendulum in Figure 1b. Likewise, the kinetic and potential energies of the clock pendulum would only occupy a discrete set of specific values denoted by $\{T_0, T_1, T_2, T_3, T_4\}$ and $\{V_0, V_1, V_2, V_3, V_4\}$ respectively but wherein, due to the conservation of energy principle, $E_{\text{pen}} = T_j + V_j, \forall j$. Moreover, if the allowable sets of kinetic and potential energies were modeled as countably finite rather than countably infinite with N allowable pairs, $\{T_0, T_1, T_2, \dots, T_{N-1}\}$ and $\{V_0, V_1, V_2, \dots, V_{N-1}\}$, then the energies could be modeled as discrete N -dimensional vectors. In fact, the total energy of the clock pendulum, whether modeled as a continuous or a discrete harmonic oscillator is the well-known Hamiltonian energy operator of the pendulum since it is the sum of its kinetic and potential energies. As will be described more fully in the following sections, if the size of the pendulum were reduced to be on the order of an atomic particle, Schrödinger's equation would emerge that dictates the temporal and spatial evolutions of this idealized and quantized "quantum" pendulum oscillator in terms of its Hamiltonian.

The Hamiltonian can take on many different forms and is more properly considered a mathematical operator, \widehat{H} . Considering the continuous model of the pendulum in Figure 1, we could express the instantaneous kinetic energy to be $T_{\text{pen}} = \frac{1}{2}mv^2$ where m is the point mass modeling the pendulum and v is its instantaneous speed or magnitude of the velocity vector. Likewise, we could model its potential energy to be $V_{\text{pen}} = mgz$ where g is the magnitude of the constant force of gravity pulling the pendulum down toward the

vertical position and z is its vertical distance above the x -axis. In this case, the Hamiltonian is time-varying, $\widehat{H} = \frac{1}{2}mv^2 + mgz$, since the two observable characteristics, speed (or momentum since the mass, m , is constant) and vertical distance, are functions of time, $v(t)$ and $z(t)$. This Hamiltonian could be rewritten in terms of the pendulum's momentum, $p = mv$, as $\widehat{H} = \frac{p^2}{2m} + mgz$. In this case, the "state" of the pendulum is uniquely specified by the pair of measurable values, or observables[‡], $\{p, z\}$.

In the case of the discrete harmonic oscillator model with a countable number of observables, N , the Hamiltonian is likewise $\widehat{H} = \frac{p_j^2}{2m} + mgz_j$ where the observables are the pair $\{p_j, z_j\}$ for any of the j^{th} discrete observable values. We can express the state of the quantum system with an N -dimensional vector for either the observable p_j or z_j and since these values are fixed for a given total energy, E_{pen} , the N -dimensional state vector can be of the form of a unit-normed vector with $N - 1$ zero-valued components and single unity- or one-valued component corresponding to a particular value of p_i or z_i . We observe that the collection of all possible such state vectors form an orthonormal basis of an N -dimensional vector space. Thus, for the particle-sized generalization of the pendulum, a quantum harmonic oscillator model results with the state of the particle-sized pendulum being represented as an element in the N -dimensional vector space element known as the system (or "pendulum") state vector.

2.3 Matter Waves

The mechanical clock pendulum example is a macroscopic entity with a mass, m , comprised of an enormous number of particles and hence, it better obeys Newton's theory of motion that express its observable characteristics such as position, speed, energy and momentum as deterministic variables in the continuum. One way to consider whether the quantum theory versus Newton's theory should be used to model a system, or more precisely, the 'degree' to which QM versus Newton's theory should be used, is to consider de Broglie's matter waves [7] and the uncertainty principle [16, 17]. de Broglie's 1924 work resulted in the concept that all matter comprised of mass has a wave-like property which coincidentally also implied that zero rest mass particles such as a photon likewise have properties normally considered only for objects with mass, such as momentum. de Broglie's formula equated a particle's wavelength, λ , to the ratio of Planck's constant, h , with the particle's momentum, p , or $\lambda = \frac{h}{p}$. Due to the extremely small magnitude of Planck's constant, $h \cong 6.62607015 \times 10^{-34}$, this formula results in a wavelength of a small object with a macroscopic mass, such as a toy

[‡] An "observable" is a measurable characteristic of a system where the outcome of the measurement, or observation, is represented by a real value such as speed v , momentum p or height in the vertical, z .

marble, being more than 20 orders of magnitude smaller than the statistical/empirical average radius of a hydrogen atom, clearly an imperceptible and practically immeasurable length. However, as the mass or momentum of an object decreases to a very small magnitude, the de Broglie wavelength becomes a significant characteristic.

In considering such particles of tiny scale, the wavelike nature becomes much more dominant leading to the concept of the particle's "wave function" that can be expressed in terms of its measurable characteristics, or quantum observables, such as position, momentum and others as dependent variables. The values of these measurable characteristics are obtained by applying an observable operator to either the functional form, or, the N -dimensional quantum state vector form of the wave function resulting in a real-valued quantity as the measurement outcome or observation. When the observable operators are in the form of a matrix, their application to the wave function state vector results in a real-valued measurement outcome that happens to be an eigenvalue of the corresponding operator matrix. Furthermore, the uncertainty of such observables, before measurement, becomes significant as well.

2.4 Uncertainty

Conjugate variables obey a generalized uncertainty principle that can be derived using basic statistical principles of distributions of random variables in view of their Fourier transform relationship. Alternatively, if two observables of a system are related as a Fourier transform pair, they are said to be "conjugate variables." For particles at the quantum scale, the matter-wave relationship results in observables taking the form of random variables of a distribution due to the wave-like nature causing them to be 'spread' out, or to have variance, σ^2 . The generalized uncertainty expression provides a lower bound on the product of the standard deviations, σ , of the distributions of a conjugate variable pair and is provided in Equation 1 for the example conjugate variable observables in functional form, \hat{x} and \hat{p}_x , where the angle bracket notation is equivalent to the statistical expected value operator of a random variable, A , or $E\{A\} = \langle A \rangle$. The constant i is the 'imaginary number' satisfying $i^2 = -1$.

$$\sigma_x \sigma_p \geq \left| \frac{1}{2i} \langle \hat{x} \hat{p}_x - \hat{p}_x \hat{x} \rangle \right| \quad (1)$$

The expression, $\hat{x} \hat{p}_x - \hat{p}_x \hat{x}$, indicates the commutative relationship among the example observables, \hat{x} and \hat{p}_x . When these observables are conjugate variables, they do not commute in general. A commonly used operator is the "commutator" denoted with square brackets and defined in Equation 2.

$$[\hat{x}, \hat{p}_x] \equiv \hat{x} \hat{p}_x - \hat{p}_x \hat{x} \quad (2)$$

The generalized uncertainty relation of Equation 1 can be rewritten in terms of the commutator as given in Equation 3.

$$\sigma_x \sigma_p \geq \left| \frac{1}{2i} \langle [\hat{x}, \hat{p}_x] \rangle \right| \quad (3)$$

One of the axioms of the theory of QM is the “canonical commutation” relation that states the $N \times N$ -dimensional operator matrices, $\hat{\mathbf{X}}$ and $\hat{\mathbf{P}}_X$, that are equivalent to the functional forms, \hat{x} and \hat{p}_x , of the observable operators for a conjugate pair are non-commutative and their commutativity relationship is equal to a constant. In terms of the position observable operator, $\hat{\mathbf{X}}$, and the momentum operator expressed as a function of the position basis, $\hat{\mathbf{P}}_X$, the canonical commutation relation is given in Equation 4 where \mathbf{I}_N is the $N \times N$ identity matrix.

$$[\hat{\mathbf{X}}, \hat{\mathbf{P}}_X] = i2\pi h \mathbf{I}_N = i\hbar \mathbf{I}_N \quad (4)$$

The canonical commutation relation is attributed to Heisenberg, Born and Jordan who are pioneering founders of the theory of QM and serves, in part, as a definition of QM theory. When the generalized uncertainty principle of Equation 3 is combined with the canonical commutation axiom, in Equation 4, we arrive at the so-called “Heisenberg uncertainty principle” given in Equation 5 where σ_x is the standard deviation of the position conjugate variable and σ_p is the standard deviation of the momentum conjugate variable.

$$\sigma_x \sigma_p \geq \frac{\hbar}{2} \quad (5)$$

For macroscopic-sized objects, such as the toy marble, the de Broglie wavelength is so tiny, that the marble’s wave function approaches a volume that is, for all practical purposes, a miniscule collection of single points in space, thus the uncertainty of its position or momentum is extremely tiny and approaches zero. This means the toy marble and the mechanical clock pendulum has fixed or constant localized positions and momenta at any instant in time and there is no perceptible uncertainty in either measurable characteristic. However, when the particle is small, its wave function, expressed in terms of the position basis, can become significantly ‘spread out’ in terms of its position and likewise, when its wave function is expressed in terms of momentum, there is a similar ‘spread’ or, more formally, variance among the collection of points. This causes the canonical commutation value of $[\hat{\mathbf{X}}, \hat{\mathbf{P}}_X] = i\hbar \mathbf{I}_n$ to become significant and leads to oft-used descriptions such as “the position of an atomic particle is considered to exist as a probability point cloud.”

This description of de Broglie’s matter waves and Heisenberg’s uncertainty along with Schrodinger’s wave equation can be used to rigorously define QM theory and we shall not go further into this development, rather our goal is to provide enough background to the MVL community such that the remainder of this paper is easily accessible. However, one more important point remains, and that is to clarify the behavior of conjugate variables of quantum particles. When a particle’s mass/momentum is small enough that these quantum mechanical characteristics are non-negligible, then observables such as position and momentum become discrete and are no longer accurately modeled within the continuum such as would be due to Newton’s theory of motion. Furthermore, its characteristic observables, when extracted from its wave function through the application of an observable operator, such as \hat{x} or \hat{p}_x that signify position and momentum respectively, become significant in terms of Heisenberg’s uncertainty. In fact, an application of \hat{x} to the wave function will result in a single real-valued position point as a result of the measurement, but it will also likewise cause the uncertainty of its conjugate variable momentum, if it were to be subsequently measured by applying \hat{p}_x to the same wave function, to have a much larger spread of possible outcomes. Thus, the standard deviations of these observables, σ_x and σ_p , vary inversely with one another and their respective observables, position and momentum, are said to be conjugate variables. Conjugate variables, when extracted from wave functions via the application of observable operators such as \hat{x} or \hat{p}_x , are those that are Fourier transform pairs of their respective wave functions and they furthermore have statistical distributions whose variances change inversely with respect to one another due to the application of observable operators.

2.5 Information Encoding with Conjugate Variables

While the uncertainty, wavelike and discrete nature of observables of quantum particles, such as photons, may seem to be unsettling at first, it is precisely these relationships that enable the promise of QI to overcome many of the limitations present in classical systems such as classical electronic circuits leading to the so-called “quantum advantage.” The discrete nature of quanta allows for the use of an inherent and natural quantization for artifacts based on QM as contrasted to defining continuous voltage, current or charge ranges and assigning a “logic” value to them as is done in classical electronic switching circuits. The probabilistic nature of measuring observables that results from uncertainty likewise leads to the extremely powerful concept of “information parallelism” through “quantum superposition.” By constraining quantum engineering artifacts to confine the observables to only two possible wave function basis states, we can assign a logic value of zero, $|0\rangle = [1 \ 0]^T$, to first state and a logic value of one, $|1\rangle = [0 \ 1]^T$, to the

second state resulting in a quantum bit or “qubit.” Due to the uncertainty principle, a qubit can be represented by a quantum particle’s wave function, Ψ , that is expressed as a function of one of its conjugate variables and described as a two-dimensional vector since only two allowable states are considered, $|\Psi\rangle = [\alpha_0 \ \alpha_1]^T = \alpha_0 |0\rangle + \alpha_1 |1\rangle$. The wave function, $|\Psi\rangle$, can thus represent both zero and one simultaneously with some a priori probability of the outcome of their measurements – this is “information parallelism” or “quantum superposition.” However, there is no inherent reason that engineering artifacts must be limited to only two states, it is theoretically just as easy to build artifacts that limit the states to $N > 2$ states[¶] for some of the conjugate variables of a photon resulting in quantum digits, or “qudits,” rather than qubits as shown in Equation 6. Such higher-dimensional quantum systems, particularly when the observables of a photon encode information, are thus the subject of the following portions of this paper.

$$|\Psi\rangle = \sum_{j=0}^{N-1} \alpha_j |j\rangle \quad (6)$$

Specifically, we consider a photon’s location, frequency, polarization and spatial angular momentum observables for the purpose of representing information in a QPIC. These characteristics correspond to the position, energy, and momentum conjugate variables and thus are subject to existing in a state of superposition among a discrete set of basis wave functions due to their uncertainty and wavelike behaviors that, in turn, offer the promise of a quantum advantage. We note that other measurable characteristics could also be used to encode information, but we focus on these four examples here. Finally, we also note that use of the photon as a carrier of quantum information offers a very important practical engineering consideration in that it is the only quantum information carrier that does not require an extreme degree of refrigeration to retain coherence; thus, offering the advantage to design and fabricate QI artifacts that operate at room temperature.

3 QUANTUM PHOTONIC POLARIZATION ENCODING

Historically, quantum photonics has embraced the exploitation of the state of polarization of a photon as a primary carrier of information. Although

[¶] “Theoretical ease” does not imply ease in engineering development, more supporting components are generally required to support higher-dimensioned quantum systems in engineering artifacts; however, such higher-dimensioned artifacts have been produced and it is currently an active area of engineering research to determine if higher-dimensioned quantum artifacts will ultimately dominate – this is one of the points of this paper.

the intention of this paper is to survey higher-dimensioned quantum photonic information encoding for the multiple-valued logic community, the widespread use of photon polarization as an information carrier, which is naturally limited to a binary basis, is included in this section for both completeness as well as to provide context for polarization-based QPIC implementation issues. Furthermore, as will be discussed in this section, the use of polarization-encoding can augment other forms of N -dimensional conjugate variable encoding to enable a doubling of the dimension or radix to yield a $2N$ -dimensional hybrid-encoded QPIC.

The use of photon polarization for information encoding allows a single photon's wave function to be expressed in terms of two orthogonal polarization basis vectors, $|h\rangle$ and $|v\rangle$, where polarization is a manifestation of the temporal angular momentum conjugate variable of the wave function. Thus, a single photon with polarization-based information encoding results in a two-dimensional state vector or qubit. This is observed to be the case since the photon's direction of propagation is given by its instantaneous Poynting vector and the corresponding state of polarization is entirely described within a plane perpendicular to the Poynting vector. Therefore, the polarization basis comprises any two chosen orthogonal vectors within the plane that we generally refer to here as $|h\rangle$ and $|v\rangle$. We note that polarization should not be confused with the spatial angular momentum conjugate variable of a photon, manifested as "orbital angular momentum" (OAM) and discussed more fully in Section 6, does not suffer from this binary basis limitation and does allow for higher dimensioned QI applications. In fact, the dimensionality of OAM encoding may be doubled in some QI applications by augmenting it with the polarization encoding discussed here.

In a tabletop bulk optics realization of a QI artifact, polarization-encoded qubits are a sensible choice. Traditionally a variety of key QI components or 'gates' were realizable using the polarization observable and hence the photonic circuitry for important early quantum computing algorithms and communications protocols was able to be physically constructed and demonstrated [18–24].

For many reasons, an overwhelming majority of photonic integrated circuits to date have been based on the use of rectangular cross-sectional waveguides to constrain the direction of EM propagation that is predominantly single mode and hence, only supports a single polarization basis. While these rectangular cross-section waveguide dimensions and the contrast of the indices can allow higher order EM modes, these higher-order modes come with significant loss and group velocity differences between modes. However, waveguides of square cross section allow for degenerate modes with equal loss and group velocity, and these modes in superposition provide an on-chip approach to forming and stably propagating any state of polarization.

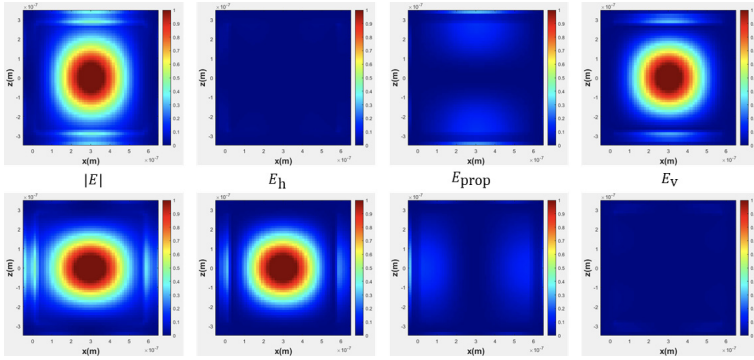


FIGURE 2
Electric Field Components Vertically/Horizontally Polarized Lower Modes

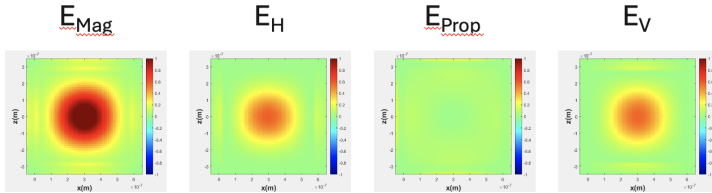


FIGURE 3
Amplitude and Phase of $h + v$ Mode.

Changing the cross-sectional waveguide to one with a square cross-section introduces a symmetry that allows for a wide range of QI applications based on polarization including polarization-encoded qubits. Furthermore, careful breaking of the square symmetry allows for realizing a variety of useful components or “gates” that evolve the photonic wave function to a new state and that may be arranged as a quantum circuit within QPICs to realize algorithms. Importantly, the square waveguides and their variations that provide components may be fabricated with the same standard photolithographic techniques that are used in electronic semiconductor foundries [24].

Figure 2 shows the electric field components for the vertically polarized and the horizontally polarized lowest order modes in the proposed square cross-sectional waveguide. To avoid confusion, these respective mode components are labeled relative to the invariants of the photonic integrated circuit (PIC) geometry envisioned herein, namely horizontal, h , vertical, v , and for the direction of propagation, prop. As verified numerically, these modes are orthogonal. Further, linear combinations of the h and v modes also propagate at the same velocity as the individual h and v modes. Figure 3 shows the amplitude and phase plots of an $h + v$ mode.

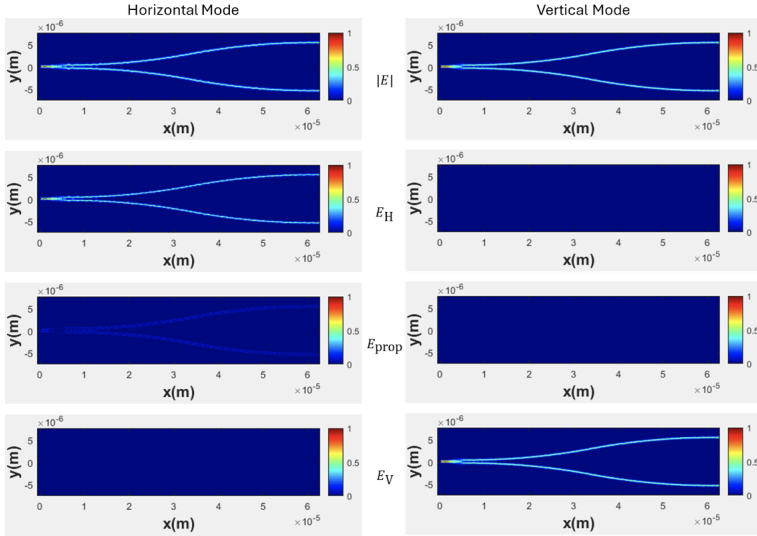


FIGURE 4
Propagation of h and v Modes Through Typical Y-coupler.

The degeneracy of the h and v modes result from the square symmetry of the waveguide and gives rise to utility, particularly in the context of polarization encoding of single and few-photon QI applications. Judicious breaking of this symmetry enables further utility in the form of polarization-sensitive components. For example, curving, narrowing or widening the waveguide in one dimension, or placing additional waveguides parallel to the first waveguide affects the two modes differently.

Not all broken symmetries distinguish significantly between h and v mode components. Figure 4 shows the propagation of the h and v modes through a typical Y-coupler component, although redesigned for waveguides with square cross-sections. In QI, the ability to equally split single photons of arbitrary polarization is useful and represents the operation of evolving a basis state into a state of superposition. The Bell inequality test for quantized behavior, for example, is widely deployed for this purpose. Homodyne detection for enhanced signal-to-noise ratio (SNR) is another application. In the Y-coupler shown, the v -mode splitting is perfectly symmetric with -3.30 dB in each branch. The h -mode is mildly asymmetric with -3.35 dB in the top branch and 3.31 dB in the bottom branch.

Conversely, a mode splitter – a polarizing beamsplitter or Hadamard operator from a QI point of view – may be realized using two closely spaced parallel waveguides, because the v -mode exhibits stronger coupling than the h -mode. Figure 5 shows a top view of the coupling behavior of two parallel

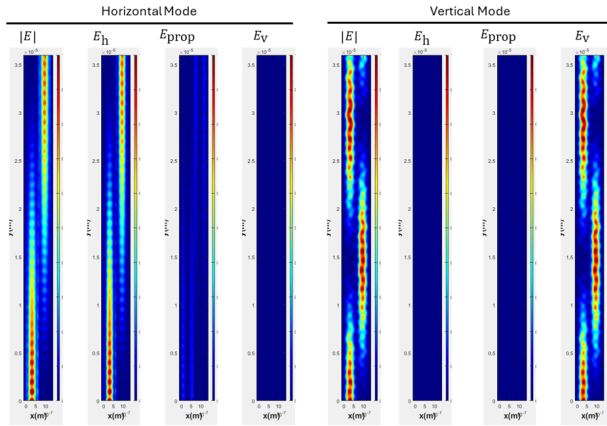


FIGURE 5
Electric Field in Waveguides After Mode Splitting.

550 nm \times 550 nm square Si/SiO₂ waveguides separated by 100 nm. The v mode couples quickly with a coupling period of $\sim 13.5 \mu\text{m}$, compared with a coupling period of $\sim 37.5 \mu\text{m}$ for the h mode. Interestingly, good crosstalk-free v -mode coupling occurs at three periods. At this point, 97% of the v mode and 1% of the h -mode are coupled with a loss of 2%.

By adjusting the spacing and the total interaction length, equal splitting for both modes may be simultaneously achieved. One example of suitable dimensions for this component is a 75 nm gap between the two parallel waveguides with a $\sim 38 \mu\text{m}$ coupling length. The modes for this splitter are less distorted than those computed for the Y-coupler results shown in Fig. 3-3.

A ‘microring resonator’ (MRR) evanescently coupled to a waveguide is often used for the nonlinear optical production of entangled signal-idler photon pairs since it can induce a four-wave mixing (FWM) process. Evanescent coupling for more complicated geometries is, however, made more difficult by the different interaction lengths. It is challenging, for example, to find a robust design for a MRR that supports both h mode and v mode FWM operations equally. One challenge is to balance the coupling that is different for the two orthogonal modes. However, with the mode splitter shown in Fig. 3-4, single mode MRRs may be used. Furthermore, two separate single mode MRRs may be implemented – one on each of the two output waveguides of the mode-splitter in Fig. 3-4.

A further example of a polarization component that can be realized in a square waveguide geometry is a $\lambda/2$ waveplate based on a taper. Since the effective index of a square waveguide is a function of the dimensions of the waveguide, tapering in one direction provides a different propagation speed

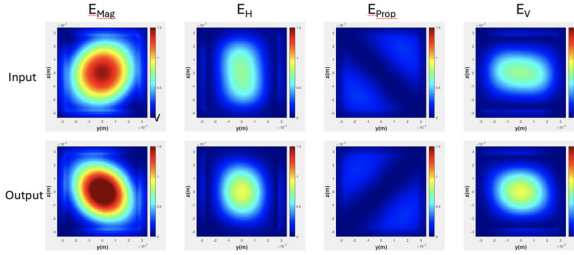


FIGURE 6
Input and Output Mode Character of V-shaped Taper.

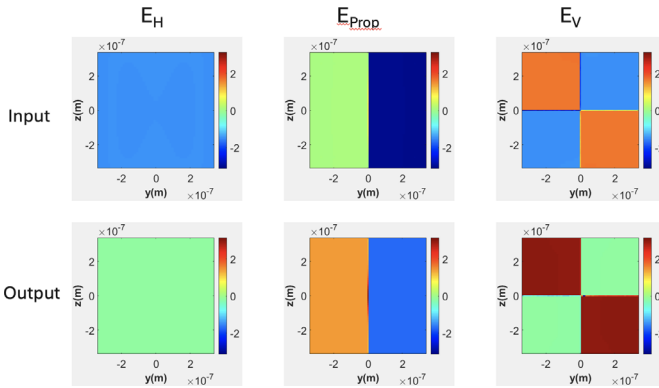


FIGURE 7
Electric Field Phases at Input and Output of Taper.

for the h -mode relative to the v -mode thus imparting the action of a waveplate with polarization encoding. Using this break in symmetry introduces a π -phase shift (180°) between the h mode and the v mode which is equivalent to a Pauli- Z operation in terms of QI. Figure 6 shows the input and output mode character of a V-shaped taper. In Figure 6, the horizontal width of the waveguide first tapers down to 400 nm within a length of $7.5 \mu\text{m}$ and then increases back up to 550 nm within a second $7.5 \mu\text{m}$ length of expanding taper. The input mode in Figure 6 is a 50:50 superposition of h -mode and v -mode components thus representing the generation of quantum superposition in a polarization-encoded qubit. The output is also an equal mixture of h -mode and v -mode, but with the phase difference rotated by 90° , which implements an S -gate for a superimposed polarization-encoded qubit. The loss in this waveplate is $\sim 1\%$.

Figure 7 shows the phases of the electric fields at the input and the output of the taper.

Coupling on and off the PIC has also been addressed. Edge couplers that transition between a fiber and a waveguide can also be designed. Interestingly, coupling losses for a typical (circular shaped) SMF-28 fiber optic cable to a square Si waveguide can be a factor of 5 or more times smaller than for a comparable rectangular waveguide. Symmetry, here too, plays the key role in this improvement as it is apparently easier to approximately ‘square a circle’ than to ‘rectangle a circle.’

Thus, it is both possible and useful to design and fabricate square waveguides whose symmetry allows stable, dispersion-free propagation of polarization-encoded qubits. In addition, a variety of integrated couplers, waveplates and polarizers can be realized. A qubit encoded in polarization in a square waveguide may thus be written as a superposition of a horizontal and a vertical component, $|\Psi\rangle = \alpha|h\rangle + \beta|v\rangle$ as it is in free space polarization-encoding and processing. Similarly, the components described here allow analogs of diagonal basis states $|\pm\rangle = \frac{1}{\sqrt{2}}(|h\rangle \pm |v\rangle)$ and by retarding the phase of one of the components, with circular polarization $|\frac{L}{R}\rangle = \frac{1}{\sqrt{2}}(|h\rangle \pm i|v\rangle)$, which corresponds to a QI S-gate operation. This set of bases encoded in polarization follows exactly those used in free space polarization-based processing. With this advance it is possible to double the number of logical levels from N to $2N$ by using polarization in an integrated photonic architecture since it can augment another independent conjugate variable, such as the location-encoded variable that has N bases [24].

4 QUANTUM PHOTONIC LOCATION ENCODING

As previously discussed, rectangular cross-sectional waveguides are typically employed within a QPIC to constrain the position and propagation direction of a photon although we provided new results regarding the use of square cross-sectional waveguides. Independently of the shape of the waveguide, when it is desired to use the position conjugate variable only to represent information, N multiple waveguides can be implemented within the QPIC and labeled as corresponding to different position basis states of a single photon’s wave function. When $N = 2$, the binary case, the QPIC supports qubits and location encoding is sometimes referred to as “dual-rail encoding,” due to the structural similarities among a QPIC and ASIC that employs differential-mode electrical signaling. When $N > 2$, the location-encoded QPIC supports qudits that are represented as higher dimensioned quantum state vectors. This multiple waveguide implementation can support the propagation of a photon when it exists in a quantum superposition with respect to its position observable. Regardless of the value of N , this form of quantum information encoding within a QPIC is referred to by various names including ‘path encoding’

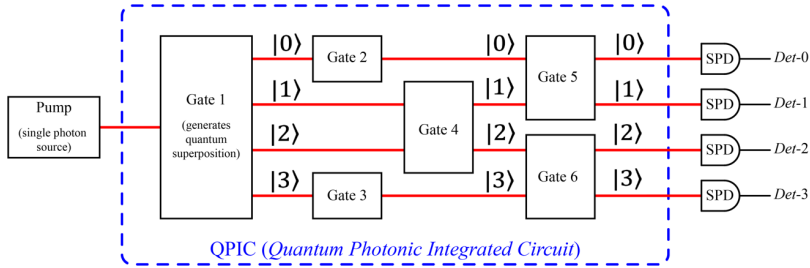


FIGURE 8
Diagram of Location-encoded QPIC with External Pump and Detectors.

and ‘location encoding.’ The common theoretical principle for this form of information representation in a QPIC is the exploitation of the wave function’s position conjugate variable to represent and process quantum information. Figure 8 contains a diagram of a single photon location-encoded QPIC that implements four-dimensional, $N = 4$, qudits with an external single photon source, the “pump,” and four external “single photon detectors (SPD) for each basis state. The red lines represent waveguides and fiber optic cables. The red lines that are external to the QPIC boundary, from the pump output to the leftmost edge of the QPIC and from the rightmost edge of the QPIC to the input of the SPD devices, are fiber optic cables that connect to the QPIC substrate via input/output edge couplers on the QPIC package. The red lines internal to the QPIC are waveguides that are each annotated with the location basis vectors they represent, $|0\rangle$ through $|3\rangle$. The external SPD are devices that convert the energy present in a photon wave packet into an electrical pulse; thus, the solid black lines that represent the SPD outputs are electrical conductors that drive the signals *Det-0*, *Det-1*, *Det-2*, and *Det-3*.

To illustrate how the use of N waveguides on a QPIC encodes information via the position conjugate variable, we first give the general form of a single photon wave function as the photon is propagating in free space and then compare it to the form of the wave function when it is constrained to propagate within $N = 4$ waveguides implemented on a QPIC such as that in Figure 8. This wave function is the generalized solution to Schrödinger’s wave equation with the initial condition that the photon is located at the three-dimensional spatial coordinate system origin, $\mathbf{r}_0 = \mathbf{0}$, at time, $t = 0$, where $\mathbf{0}$ is the three-dimensional null vector. Equation 7 shows the wave function, $\Psi(\mathbf{r}, t)$, in traditional linear algebraic notation where non-italicized bold font indicates a vector and italicized non-bolded font indicates a complex-valued scalar. In Equation 7, the position of the photon at time, t , is indicated by a real-valued three-dimensional spatial vector, $\mathbf{r}(t)$, in units of meters, the spatial frequency or angular wave vector, \mathbf{k} , with units of radians per meter and

the temporal wave frequency, ω , in units of radians per second. Without loss of generality, the wave functions in this Section are given with a phase angle offset of 0° .

$$\Psi(\mathbf{r}, t) = |\Psi(\mathbf{r}, t)\rangle e^{i(\mathbf{k}\cdot\mathbf{r}-\omega t)} \quad (7)$$

Likewise, this same wave function is expressed in Dirac's 'braket' notation in Equation 8.

$$|\Psi(|r\rangle, t)\rangle = \langle\Psi|\Psi\rangle e^{i((k|r)-\omega t)} \quad (8)$$

In Equations 7 and 8, the wave functions are written in terms of the position conjugate and the photon can be intuitively considered as simultaneously existing in a plurality of three-dimensional free-space locations specified within some uncertainty volume whose position is indicated by the $\mathbf{r} = |r\rangle$ random position vector before it is measured. More specifically, the photon is probabilistically present within a volume whose location is indicated by $\mathbf{r} = |r\rangle$ in accordance with the probability distribution, $|\Psi(\mathbf{r}, t)|^2 = \langle\Psi|\Psi\rangle$, and with a standard deviation of $\sigma_{\mathbf{r}} = [\sigma_x \ \sigma_y \ \sigma_z]^T$ in accordance with the uncertainty relation in Equation 5. In this case, the wave function is of the form of a three-dimensional vector whose component wave functions are each in terms of the projection of the general form in Equations 7 and 8 with unit vectors along each axis of the coordinate system defining the position vector $\mathbf{r} = |r\rangle$. These explicit component wave functions are provided in Equations 9, 10 and 4-5 where $\mathbf{r} = |r\rangle = [r_x \ r_y \ r_z]^T$ is used to indicate the components of the position vector projected to the unit vectors defining the coordinate system, or free-space position basis, $\{\mathbf{u}_x, \mathbf{u}_y, \mathbf{u}_z\} = \left\{ [1 \ 0 \ 0]^T, [0 \ 1 \ 0]^T, [0 \ 0 \ 1]^T \right\}$.

$$\Psi_x = \langle\Psi_x|\Psi_x\rangle e^{i(k_x r_x - \omega t)} \quad (9)$$

$$\Psi_y = \langle\Psi_y|\Psi_y\rangle e^{i(k_y r_y - \omega t)} \quad (10)$$

$$\Psi_z = \langle\Psi_z|\Psi_z\rangle e^{i(k_z r_z - \omega t)} \quad (11)$$

In contrast, when the photon is constrained to propagate along the axis of one of $N = 4$ waveguides implemented within a QPIC, as depicted in the diagram of Figure 8, its wave function is likewise a solution of Schrödinger's wave equation as in the free-space case but with boundary conditions imposed by the spatial geometries of the $N = 4$ waveguides as well as the initial conditions. In this case, the wave function can be expressed as a four-dimensional

vector, $|\Psi\rangle$, in terms of the waveguide labels that are present in the four-dimensional vector $|z\rangle$ as annotated in Figure 8. We choose the variable “ z ” to represent the axial directional axis of a waveguide since each waveguide constrains the location of the photon to be contained within their interior boundaries due to the idealized total internal reflection occurring at the cross-sectional waveguide boundaries and thus having a net propagation direction, Poynting vector, in the axial or “ z -direction,” of each waveguide. Thus, the wave function is still dependent upon a position conjugate variable, it just happens to be constrained to lie along the one-dimensional path defined by the z -axis of each waveguide due to its spatial geometry as placed and routed on the QPIC substrate. It is unnecessary to use actual spatial coordinates related to the physical position of each waveguide’s z -axis, it is only necessary to define a four-dimensional orthonormal basis vector set such that each independent basis vector is attributed to one of the $N = 4$ waveguides and that represents a position coincident with each waveguide’s axial path of wave function propagation. Conventionally, the canonical four-dimension “computational basis” is used, $|z\rangle \in \{|0\rangle, |1\rangle, |2\rangle, |3\rangle\} = \left\{ \begin{bmatrix} 1 & 0 & 0 & 0 \end{bmatrix}^T, \begin{bmatrix} 0 & 1 & 0 & 0 \end{bmatrix}^T, \begin{bmatrix} 0 & 0 & 1 & 0 \end{bmatrix}^T, \begin{bmatrix} 0 & 0 & 0 & 1 \end{bmatrix}^T \right\}$. Equation 12 contains the wave function expressed in terms of the $N = 4$ waveguides’ position variable, $|z\rangle$. Although Equation 12 is similar in structure to Equation 8, the wave function of Equation 12 is four-dimensional since $N = 4$ waveguides are used rather than the three-dimensional free-space wave function of Equation 8.

$$|\Psi(|z\rangle, t)\rangle = \langle\Psi|\Psi\rangle e^{i(k|z\rangle - \omega t)} \quad (12)$$

Each component of the four-dimensional vector in Equation 12 represents the orthogonal wave function component of the photon as it propagates through the $N = 4$ waveguides as given in Equations 13 through 16 where the wave number, k , is assumed constant for all components since the same waveguide fill material is used for all waveguides fabricated on a QPIC, thus the spatial frequency, k , is the same for each waveguide.

$$\Psi_0 = \langle\Psi_0|\Psi_0\rangle e^{i(kd_0 - \omega t)} \quad (13)$$

$$\Psi_1 = \langle\Psi_1|\Psi_1\rangle e^{i(kd_1 - \omega t)} \quad (14)$$

$$\Psi_2 = \langle\Psi_2|\Psi_2\rangle e^{i(kd_2 - \omega t)} \quad (15)$$

$$\Psi_3 = \langle\Psi_3|\Psi_3\rangle e^{i(kd_3 - \omega t)} \quad (16)$$

The real scalar values $\{d_0, d_1, d_2, d_3\}$ in Equations 13 through 16 represent the distance along each waveguide that the wave function has propagated since the initial condition for the time variable, t_0 , to the current time, t . We note that the relationship, $d = v_p t$, is used to express the distance, d , the wave function has propagated since the initial time condition, t_0 , as the product of the phase velocity, v_p , with the current time variable, t . Because the wave function is injected into the input ports of the $N = 4$ waveguides at the same instant of time, $d_0 = d_1 = d_2 = d_3 \equiv d = v_p t$, and Equations 13 through 16 can be rewritten by substituting each kd_j term for all $j \in \{0, 1, 2, 3\}$ with $kv_p t$, thus causing all the exponential terms to become identical as $e^{i(kv_p t - \omega t)} = e^{i(kv_p - \omega)t}$. Therefore, the only distinguishable differences among the wave function components for the $N = 4$ waveguides, are complex scalars that multiply each exponential term, $\{\Psi_0, \Psi_1, \Psi_2, \Psi_3\}$ that are known as the "probability amplitudes" of the wave function.

The quantum state vector for the $N = 4$ waveguides QPIC is given in Equation 17 and is simplified given the previous observation that it is the four-dimensional wave function vector in terms of the waveguide label or location variable, $|z\rangle$. In this example, $|z\rangle$ is represented by the computational basis, $\{|0\rangle, |1\rangle, |2\rangle, |3\rangle\}$, as is typical in QI applications and the $e^{i(kv_p - \omega)t}$ term is assumed to be present, but suppressed since it is identical in each orthogonal component of the wave function as shown in Equation 17.

$$|\Psi\rangle = \Psi_0 |0\rangle + \Psi_1 |1\rangle + \Psi_2 |2\rangle + \Psi_3 |3\rangle \quad (17)$$

Due to uncertainty in the position conjugate, $|z\rangle$ is a random vector with probability mass function $\langle\Psi|\Psi\rangle$. Each complex-valued probability amplitude scalar, Ψ_j , in Equation 17 can be used to compute the probability that the wave function collapses to a single waveguide, or position observable, during a measurement as shown in Equation 18.

$$\text{Prob}\{\text{event that photon localizes to waveguide } |j\rangle\} = \Psi_j^* \Psi_j = |\Psi_j|^2 \quad (18)$$

When the photon is in a state of superposition with respect to its position conjugate, we can abstractly consider the single photon to be spatially present within all four waveguides simultaneously and this is indicated when more than one probability amplitude of Equation 17 is non-zero. Of course, a measurement of a superimposed photon wave function results in observing the photon to be present in a single waveguide, $|m\rangle$, with probability as given in Equation 18, and the quantum state vector evolves into a single basis state due to the measurement indicated by $\Psi_m = 1$ and $\Psi_j = 0, \forall j \neq m$.

Initially, photons must be generated and injected into the location encoded QPIC and this is typically accomplished by coupling a source, or “pump” to a single waveguide within the QPIC as shown on the leftmost side of Figure 8 which clearly represents a corresponding quantum state as a single basis state or collapsed form, $|\Psi\rangle = |m\rangle$, where m is any arbitrary waveguide position basis vector with a probability amplitude of unity (one). It is generally the case that the wave function must be evolved into a state of superposition to derive any quantum advantage with respect to the processing method embodied within the QPIC; this requires the implementation of a QPIC component or gate that transforms the single basis state into a superimposed state. Such a gate is represented in Figure 8 by the box labeled “Gate 1.” In principle, there are a variety of such components that could be used to accomplish the generation of a superimposed wave function, or state vector, with the only requirement being that they are realizable and capable of being implemented as QPIC gates. One family of such theoretically possible QPIC gates are those that are characterized by transfer matrices of the form of a “complex-valued Hadamard matrix” (CHM). CHM are a family of matrices clearly of interest in QI, but for which there has also interest in other applications for over 100 years [25]. There remain unsolved questions regarding both the mathematics of CHM as well as engineering questions regarding their implementation that continue to be actively under investigation [26]. It is possible that new CHM research results will result in the availability of new and more desirable components with CHM transfer matrices for use in QPIC design. Increased interest in designing and fabricating location-encoded QPICs will likely continue to motivate this line of research.

For binary or qubit based QPICs, the well-known real-valued 2×2 Hadamard gate has a transfer matrix of, $\mathbf{H}_{\text{Had}} = \left(\frac{1}{\sqrt{2}}\right) (|0\rangle\langle 0| + |0\rangle\langle 1| + |1\rangle\langle 0| - |1\rangle\langle 1|)$, and is typically employed to generate superposition from a single basis state since it corresponds to a power-splitter or Y-coupler as discussed in Section 3. Mathematically, the Hadamard transfer matrix is the discrete Fourier transform matrix over GF(2), thereby permitting one to consider its action as transforming the input single basis state, viewed as a discrete modulo-2 Dirac delta functional, into a spread of superposition among the two dual-rail waveguides whose corresponding probability amplitude magnitudes are numerically equal. When the magnitudes of the probability amplitudes are all non-zero and their magnitudes are equal in value, ‘perfect superposition’ is said to be achieved. For the higher dimensioned case, $N > 2$, the higher-radix generalization of the Hadamard gate is the Chrestenson gate with a transfer matrix denoted as, \mathbf{C}_N , that likewise represents the discrete modulo- N Fourier transform matrix [27] and is one choice for the generation of perfect superposition in a higher dimension location-encoded QPIC when the wave function is initialized to a single collapsed basis state. A recently described

QPIC gate that evolves a photonic wave function, initially in one of the four basis states, $|0\rangle$ through $|3\rangle$, into a state of perfect superposition is the radix-4 Chrestenson gate described in [28]. Mathematically, this gate would evolve a basis state of, for example, $|\Psi\rangle = |0\rangle$, into the state of perfect superposition, $|\Psi\rangle = \frac{1}{2}(|0\rangle + |1\rangle + |2\rangle + |3\rangle)$, and represents a viable choice for the QPIC component annotated “Gate 1” in Figure 8.

A measurement of the photon’s location can be implemented by coupling four distinct single photon detectors (SPD) to each waveguide as depicted in Figure 8. Clearly, since a photon is an indivisible quantum of EM energy and assuming ideal operation where the practical possibility of photon loss in the QPIC is discounted, only a single SPD will “fire” or register the presence of energy, even when the photon wave function is in a superimposed state among the $N = 4$ fiber optic cables providing input to the SPDs.

The use of additional photonic components that transform the quantum state is accomplished in a QPIC by connecting their input and output ports to one or more of the waveguides in the QPIC. Figure 8 contains some abstract example components, or gates, that are coupled to internal QPIC waveguide segments labeled as “GATE 2” through “Gate 6.” The selection, placement, and transfer functions of the gate components, some of which may be non-linear, define the functionality of the QPIC as determined by the designer. Note that the components labeled “Gate 2” and “Gate 3” are single-photon, or single qudit gates, and only couple to a single individual waveguide while others, labeled “Gate 4,” “Gate 5” and Gate 6,” are multi-photon and couple to two waveguides. Although multi-photon components may be used in the QPIC, it is emphasized that single photon qudits are being described here and the multi-photon gates function with the single photon superimposed wave function.

In terms of information representation within a location-encoded QPIC, the objective is to use some aspect of the quantum state in Equation 17 to encode information. Although a variety of different methods exist to encode information within the quantum state of a qudit [29], the most common method is “basis encoding.” Basis encoding uses the basis vector labels or values to represent information. In the four-dimensional QPIC example described here, the information is represented with a radix-four, digit set, $|z\rangle = \{0, 1, 2, 3\}$, since the position conjugate is constrained and encoded to be in the discrete computational basis set, $\{|0\rangle, |1\rangle, |2\rangle, |3\rangle\}$. In terms of QI, the quantum advantage with respect to QPIC functionality is achieved through the exploitation of QM properties such as superposition and entanglement as is true of other forms of DV quantum information processing. Higher-dimensioned entanglement among the photon wave functions [27] can be achieved, typically through using multi-photon components such as an MRR that can impart the FWM nonlinear effect and offers many

well-known and desirable advantages in QI. An example of a recently fabricated QPIC that uses a single heralded photon is a true random number generator (TRNG) as disclosed in [30] where both a binary radix and a radix-4 QPIC are described.

5 QUANTUM PHOTONIC WAVELENGTH/FREQUENCY ENCODING

Another form of the uncertainty principle states that energy, E , of a particle is a conjugate variable with respect to time, $\Delta E \Delta t \geq \frac{\hbar}{2}$, although it is noted that time, t , is not a quantum observable of a particle, rather it is an independent system variable in Schrödinger's equation. While position and momentum are measurable characteristics of a quantum particle, there is no concept of measuring a particle's 'time characteristic' nor is there an observable operator, \hat{t} . However, as discussed in Section 2, there is an observable operator for energy, E ; the Hamiltonian, \hat{H} . In fact, when the energy versus time uncertainty is discussed, Δt is generally a quantity considered to be intrinsic or inferred with respect to some other observable that does happen to be a conjugate with respect to E .

More specifically, if we assume a particle has some generalized conjugate observable \hat{q} that obeys generalized uncertainty, or in other words, is a conjugate with respect to E , then following the derivation in [15], we can express the generalized uncertainty in terms of \hat{H} and \hat{q} , followed by applying the canonical commutation axiom of QM to arrive at Equation 19.

$$\sigma_H \sigma_q \geq \frac{\hbar}{2} \left| \frac{d\langle q \rangle}{dt} \right| \quad (19)$$

Next, the definition, $\sigma_H \equiv \Delta E$, is assumed and the 'intrinsic time' term, Δt , is obtained from Equation 19 by defining it as a ratio of σ_q with respect to the first-order time derivative of \hat{q} as given in Equation 20.

$$\Delta t \equiv \frac{\sigma_q}{\left| \frac{d\langle q \rangle}{dt} \right|} \quad (20)$$

Equation 20 is essentially a mathematical definition of 'intrinsic time,' Δt , as inferred from a true observable, \hat{q} , since it relates the standard deviation, σ_q , of the legitimate particle observable, \hat{q} , with its time rate of change of its average value, $\langle q \rangle$. Observing Equation 20 clearly shows that Δt is the time interval required for the expected value of observable q to change by one standard deviation, σ_q , as normalized by its average rate of change. Because

the observable \hat{q} exists and is truly a measurable characteristic of a quantum particle, we can infer the intrinsic value of Δt .

As energy E has been established to be a conjugate variable with respect to some other observable q and the intrinsic time Δt can be inferred from \hat{q} , we can now examine the use of the E variable in more detail for the QI purposes of encoding information. With respect to a single photon, it is a well-established fact that its energy is directly proportional to its frequency, ω , in units of radians per second as given in Equation 21.

$$E = \hbar\omega \quad (21)$$

Equation 21 is the typical case for a photon of a single color; however, because its energy, E , is a conjugate variable, the uncertainty relationship holds as previously discussed and this fact enables the use of ω to encode information in the photon's quantum state or wave function. In this case, the total energy, E , of the photon is sharply known, but there is uncertainty with respect to its frequency content. The implication is that it must be possible to evolve the wave function into a state of superposition with respect its frequency observable thus producing a 'multi-colored' photon, at least prior to measurement when it will collapse into a single color. In such a case, we associate a vector basis set with each frequency or color, and the result is a QI approach generally referred to as "frequency-bin encoding" [31, 32]. We note that the overall idea of using different frequencies to represent information is not a new concept as the telecommunications industry has used this approach classically for many years, often termed "wavelength division multiplexing" (WDM) and therefore, the QPIC and QI communities can benefit from using many of the previously developed WDM devices and methods by applying them to QI applications.

In terms of the higher dimension DV QI approaches that are considered here, we design our QPIC to host and process only a fixed discrete set of allowable wavelengths. In practice, this restriction is not difficult to implement within a QPIC as single photon sources can be derived from very spectrally pure generators such as high-quality monochromatic lasers. Thus, such a laser can serve as a 'pump' that generates single-colored photons to couple into a QPIC waveguide. To preserve spectral purity of such an injected wave function, it is important that all QPIC components operate in a highly linear manner as nonlinearities can cause an injected spectral line within a wave function to generate higher-ordered terms that cause frequency harmonics to appear within the wave function.

As an example of the generation of harmonics due to a nonlinear QPIC component, assume that the nonlinear component transfer function is in the form of an operator over the wave function, $\hat{\mathbf{T}}_{\text{nl}}(\bullet)$, and is of the form of an

n^{th} -degree polynomial as given in Equation 22.

$$\widehat{\mathbf{T}}_{\text{nl}}(\bullet) = \sum_{m=0}^n a_m (\bullet)^m \quad (22)$$

For the sake of mathematical simplicity and without any loss of generality, we express the initial spectrally pure wave function as shown in Equation 23 where the spatial frequency terms and phase angles are suppressed and $|0\rangle$ is the computational basis vector that encodes the pump frequency, ω_0 .

$$\Psi_0 = |\Psi_0\rangle e^{-i\omega_0 t} \quad (23)$$

Applying the nonlinear operator, $\widehat{\mathbf{T}}_{\text{nl}}$, in Equation 22 to the initially generated single-colored photonic wave function of Equation 23 causes the spectrally pure wave function, Ψ_0 , to evolve into Ψ_τ where the subscript, τ , indicates the nonlinear component has a processing delay of τ seconds as depicted in Equation 24.

$$\begin{aligned} \Psi_\tau = & a_0 |\Psi_0\rangle^0 + a_1 |\Psi_0\rangle e^{-i\omega_0 t} + a_2 |\Psi_0\rangle^2 e^{-i2\omega_0 t} + a_3 |\Psi_0\rangle^3 e^{-i3\omega_0 t} \\ & + \dots + a_j |\Psi_0\rangle^j e^{-ij\omega_0 t} + \dots + a_m |\Psi_0\rangle^m e^{-im\omega_0 t} \end{aligned} \quad (24)$$

As is observed, the resultant wave function is polluted with harmonic frequencies of the form $\{2\omega_0, 3\omega_0, 4\omega_0, \dots, j\omega_0, \dots, m\omega_0\}$ where each harmonic of the form $j\omega_0$ is referred to as the j^{th} -order harmonic. Furthermore, these higher-ordered harmonics may not fall into the selected frequency-bins that were chosen by the QPIC designer to represent data and this could result in a frequency-bin measurement wherein the wave function collapses to a single higher-ordered harmonic that is not detectable within the QPIC and the qudit could be considered as ‘lost,’ or even worse, to be detected as collapsing into an erroneous frequency-bin. Alternatively, if the one or more of these higher-ordered harmonics did happen to coincide with a designer-selected frequency-bin for representing information, the nonlinearity could also cause a measurement to yield an incorrect result from a QI processing point of view since the probability amplitudes would be incorrect.

Since the higher-ordered harmonics are integer multiples of the original monochromatic frequency comprising the wave function in Equation 23, they are typically spaced far enough away in the frequency spectrum that bandpass filters can be applied to null them out. However, a more severe issue can occur due to the generation of “intermodulation products” (IM). IM products can arise when a multi-colored photon encounters a nonlinearity within the QPIC, that is, the wave function is superimposed among two

or more frequencies and couples to a component with nonlinear characteristics. It would be expected that a QPIC employing frequency-bin encoding would support wave functions of multi-colored photons since the objective of frequency-bin encoding is to represent different information values with different designer-selected frequencies.

Consider the example wave function, Ψ_{xy} , as given in Equation 5-7.

$$\Psi_{xy} = |\Psi_x| e^{-i\omega_x t} + |\Psi_y| e^{-i\omega_y t} \quad (25)$$

When a wave function of the form of Equation 25 encounters a nonlinear component, the two frequency components ω_x and ω_y interact and IM products are produced. If we consider only the 2nd-order term of the nonlinear operator, $a_2(\bullet)^2$, and expand the wave function Ψ_{xy} into Sine and Cosine functions by applying Euler's relation, $e^{\pm i\theta} = \cos(\theta) \pm i \sin(\theta)$, the resulting wave function component due only to the 2nd-order term of the nonlinear operator contains terms of the form $\cos(\omega_x t) \cos(\omega_y t)$, $\cos(\omega_x t) \sin(\omega_y t)$, $\sin(\omega_x t) \cos(\omega_y t)$, and $\sin(\omega_x t) \sin(\omega_y t)$. Using the trigonometric product identity, we observe that new IM product frequency terms will pollute the wave function that are of the form $\omega_x + \omega_y$ and $|\omega_x - \omega_y|$. While the "second-order IM products" (IM2) can cause problems similar to those identified with respect to higher-ordered harmonics, they also tend to fall outside the frequency range of ω_x and ω_y and can at least be eliminated by incorporating a bandpass filter into the QPIC wherein the passband excludes the IM2 products while keeping the original two frequencies of ω_x and ω_y in the filter passband

When we consider the "3rd-order IM products" (IM3), a more severe problem can occur. IM3 contains several newly-generated frequencies that can be filtered since they also fall outside the frequency band containing ω_x and ω_y , however; two of the newly generated frequencies are $2\omega_x - \omega_y$ and $2\omega_y - \omega_x$ and these frequencies tend to fall in between ω_x and ω_y and thus cannot be easily filtered. This means that the frequency-bin wave function will contain these components and thus, there will be a nonzero probability that a measurement will collapse into one of these undesired IM3 basis states. Furthermore, higher-ordered IM products continue this same pattern. The trigonometric relationships indicate that for even-valued IM products such as IM4, IM6, IM8, *etc.*, newly generated frequencies fall outside the passband of ω_x and ω_y , so the problems that even-valued IM products cause are less severe since they can be filtered. However, the higher-order odd-valued IM products such as IM5, IM7, IM9, *etc.* continue to generate frequencies that fall between ω_x and ω_y , often causing them to be impossible to filter. While frequency-bin encoded QPICs have several desirable properties that make them attractive to a designer, care must be taken to properly deal with

harmonics and IM during the basis set frequency choices as well as due to nonlinearities that are often present in components that are predominantly linear. For example, sufficiently long runs of fiber optic cable can cause harmonics and IM to form. As a designer increases the radix by including more frequencies in the basis set, more opportunities for unwanted nonlinear effects are present.

Most nonlinear effects are stronger at lower-ordered products since the scalar coefficients in Equation 22, shown as a_k , are relatively much larger in magnitude for low values of m . For this reason, a QPIC designer who is employing frequency-bin encoding will generally pay the most attention to the IM3 products since they tend to dominate the problems that occur due to nonlinearities.

Thus far, we have described the problems that can arise in frequency-bin QPICs due to nonlinear components since the nonlinearities can introduce unwanted superimposed frequencies within the wave function. However, these effects can and often are also used to the advantage of the frequency-bin QPIC designer. In the location-based encoding Section 4, we describe how QPIC components with transfer matrices in the form of Hadamard, Chrestenson, and in general, CHM matrices, are typically employed to evolve a generated photon's wave function into a state of superposition after it is initially coupled into the QPIC waveguide. The same need is present for frequency-bin QPICs since single photon sources often produce spectrally pure, single-colored photons by using high-quality monochromatic lasers. Even if this were not the case for the single photon generator, it could cause problems for the QPIC designer if the initially generated information-carrying photons did not have wave functions in a known state. For frequency-bin QPICs, it is typically the case that nonlinearities are purposely designed into the QPIC for the purpose of evolving spectrally pure single-color photon into a superposition state.

Various QPIC components have been developed and used to generate multi-colored photons, or equivalently, to evolve wave functions that are initially in a basis state into a state of superposition. In [33], a process known as "Bragg-scattering four-wave mixing" (BSFWM) is used to generate two-color photons. The apparatus consists of a 100m length of fiber optic cable that is pumped with two laser beams of unequal frequencies with the pump frequency difference dictating the difference in the resulting single photon wave function. BSFWM is a nonlinear process that manifests in components that contain structural variations and are comprised of materials with a high Kerr susceptibility coefficient, $\chi^{(3)}$, that can induce a polarization field that couples the wavelengths among two photons. While this approach is interesting, it results in a qubit since there are only $N = 2$ superimposed wavelengths in the photon's wave function and furthermore, it is not a higher dimensioned

approach. Also, this approach requires the use of a large spool of fiber optic cable to be coupled to the QPIC since the nonlinear properties of the fiber are exploited for BSWFWM in [33].

To use frequency-bin encoding within a QPIC, it is desirable to use a component that can be fabricated directly onto the device substrate that evolves a photon's wave function into a state of superposition with respect to frequency content, preferably with $N > 2$ superimposed frequencies to enable high dimensional qudits that can then be used for higher-radix QI applications. One such approach is to construct a frequency comb generator directly as a component within the QPIC circuitry.

There have been several recent results concerning QPIC-based frequency comb generators. A commonly used QPIC component for generating a frequency comb generator is the "microring resonator" (MRR) as discussed in previous Sections of this paper [34–36]. MRRs are a form of cavity that is physically constructed as a closed circular waveguide. Photons are coupled into and out of the MRR by co-locating a waveguide very near an external point of the MRR to create a "coupling region" where some percentage of pump photons in the external waveguide tunnel into (and back out) of the MRR. The circumference of the MRR is designed to be equal to an integer number of wavelengths, $n\lambda_{\text{pump}}$, of the pump photon and one of the supported resonant frequencies is then $f_{\text{res}} = \frac{1}{\lambda_{\text{pump}}}$, however; the MRR has a multiplicity of resonance frequencies. This causes a circular standing wave to develop within the MRR whereby large numbers of photons accumulate as "clumps" at certain points within the MRR.

Due to nonlinearities within the MRR, a nonlinear "four-wave mixing" (FWM) process occurs that generates multi-colored photons by converting one photon, for the case of "spontaneous FWM," or two photons for the case of "stimulated FWM," into two photons that are multi-colored. FWM in general is an effect that can occur when two or more incident photons interact with each other in a nonlinear medium that causes them to interact in such a way that they convert into two photons with changed frequency and phase values in their wave functions. The MRR photons resulting from the FWM process are time-coincident and they can tunnel out of an MRR across a suitably spaced coupling region back into a waveguide that is external to the MRR. Due to the MRR's multiple resonant frequencies, it can serve as a frequency comb generator that generates photons whose wave functions comprise a superposition of resonant frequencies that are evenly spaced in the frequency spectrum by an amount known as the "free spectral range" (FSR). Thus, the use of MRRs to promote the occurrence of FWM is an example of purposely relying upon nonlinear effects to achieve a design goal, in this case to design a frequency comb generator, within a QPIC that employs frequency-bin QI encoding. A QPIC designer can complement the MRR frequency

comb with a bandpass filter to limit the number of frequency-bins and thus set the dimension, N , to be the number of resonant MRR frequencies that fall within the filter passband to be used for QI applications. Examples of the use of MRRs for frequency-bin encoded QPICs are described in [37–40].

Another component that is typically employed to transform or evolve the wave functions of frequency-bin encoded photons is the “electro-optic modulator” (EOM). EOMs use the electro-optic effect of a material to modulate the phase term of a photonic wave function with an applied voltage that causes an electric field to exist across the material, where the applied voltage is typically in the radio frequency (RF) range [41, 42]. The EOM essentially varies the optical refractive index in a nonlinear crystal in proportion to the magnitude of the externally applied RF voltage; however, in terms of its operation in evolving the photonic wave function, it can be characterized as a purely linear device. When an EOM is driven by a RF voltage that is periodic with frequency, ω_{eom} , and the frequency component within a photon’s wave function, ω_{pump} , the EOM evolves the wave function to contain frequency components at $\omega_{\text{pump}} \pm n\omega_{\text{eom}}$. While some of the generated frequencies may fall outside the finite set of N frequencies selected by the QPIC designer to represent information, these can be removed by coupling the output of the EOM to passband filters that move energy from the unwanted frequency components back into the desired frequency components. EOMs have been available as discrete packaged components for several years and more recently miniaturized designs appropriate for implementation as QPIC components are described in [43, 44].

In terms of evolving the quantum state of frequency-bin encoded wave functions within QPICs, EOMs are frequently complemented with another structure that performs “Fourier-transform pulse shaping” (FPS). FPS components consist of a frequency-domain demultiplexer and multiplexer pair with a set of phase-shifting elements known as “pulse shapers” as shown in Figure 9 where the WDM component represents a wavelength demultiplexer or a wavelength multiplexer depending on which ports are coupled to incident photonic wave functions. The leftmost WDM essentially performs a Fourier transform by separating out the frequency components of the incident wave function coupled to its input port. The components labeled “PS” represent the pulse shaping transfer functions that modify the phase of each individual separated frequency band of the incident photonic wave function.

The FPS is coupled to a frequency-bin encoded input wave function, $|\Psi\rangle$, that is then demultiplexed in the frequency domain to separate it into its frequency-bin components such that the pulse shaper components PS apply arbitrary phase shifts to each frequency bin and then the phase-shifted frequency-bins are multiplexed back together to produce the evolved wave function, $\mathbf{H}_{\text{fps}}|\Psi\rangle$. The transfer function, \mathbf{H}_{fps} , is then ideally modeled as an $N \times N$ unitary diagonal matrix with each diagonal element representing

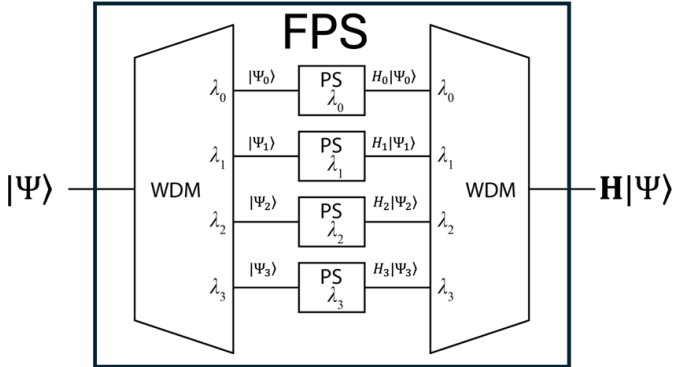


FIGURE 9
Diagram of Fourier-transform Pulse Shaping (FPS) Structure.

individual frequency-bin PS operations. Practically, the transfer matrix, \mathbf{H}_{fps} , is modeled as a cascade of the ideal unitary in cascade with a probabilistic loss transfer function to account for the case where the photon is dropped. FPS structures have been designed as QPIC components typically by using MRRs in a drop-add filter configuration [45, 46].

By implementing a cascade of alternating EOM and FPS, the so-called “quantum frequency processor” (QFP) structure results that can theoretically be used to implement any arbitrary unitary transform for frequency-bin encoded wave functions. The QFP is a powerful structure due to its generality and is scalable in terms of the QI dimension, N . Because MRR, EOM and FPS have been demonstrated as QPIC components, frequency-bin encoding is one of the more attractive options in terms of implementing frequency-bin QI applications using QPICs [38, 40, 47].

Processed photon wave functions can be detected with SPD by coupling the incident wave function to another WDM in a demultiplexing configuration with separate SPD on each output port to measure the presence of individual frequency-bin components. Alternatively, encoding translators can be used to convert the frequency-bin encoding into another form such as time-bin encoding and detector structures for those encoding methods can be used. When frequency-bin wave functions are measured directly in the frequency domain, other approaches include the use of homodyne and heterodyne detectors.

6 QUANTUM PHOTONIC SPATIAL ANGULAR MOMENTUM ENCODING

There has recently been excellent work in free space, demonstrating high dimensional quantum states using propagating photon beams that are shaped

into distributions that support “orbital angular momentum” (OAM) [48–51]. The spatial component of angular momentum, in contrast to the temporal angular momentum component or polarization of Section 3, for a given quantum state arises from the spiral nature of the traveling or propagating phase front associated with the state the net perpendicular unit vector of this surface, known as the Eikonal, rotates around the axis of propagation and this precession is the OAM. Each order, or mode index, corresponds to the number of complete rotations, also referred to as ‘the number of spirals,’ occurring within a spatial wavelength of propagation. The integer order is the photon eigenstate number, q and we can thus write a quantized angular momentum associated with q as $L = q\hbar$ [52].

OAM states are solutions to the paraxial wave equation,

$$\left[\nabla_r^2 + 2ik \frac{\partial}{\partial z} \right] \Psi(\mathbf{r}) = 0 \quad (26)$$

where ∇_r^2 is the transverse Laplacian, \mathbf{r} is the position vector, and k is the magnitude of the propagation vector \mathbf{k} . The vector \mathbf{k} is perpendicular to the average, or planar phase front, that carries the linear momentum.

The averaging nature of the of the Laplacian gives rise to a Gaussian magnitude distribution as a solution to Equation 26. In addition, this Gaussian may be modulated by a polynomial. Appropriate families of modulating polynomials are in the form of Laguerre, Ince or Hermite, and the choice of which family to use depends on the boundary conditions. OAM states are Laguerre-Gaussian (LG) states, and the order of the Laguerre polynomial is equal to the photon eigenstate number. Conveniently the Laguerre-Gaussian solutions of different order are orthogonal to each other.

Two other families of orthogonal polynomials provide solutions to Equation 26, and these are the Ince polynomials and the Hermite polynomials. Thus, each Ince-Gaussian state is orthogonal to other Ince-Gaussian states, and the same may be said for the Hermite-Gaussian family of states.

Whether a photon state should be decomposed into Laguerre-Gaussian, Ince-Gaussian or Hermite-Gaussian eigenstates depends on the boundary conditions, and the ellipticity of the appropriate coordinate system used to describe those boundary conditions. Laguerre-Gaussian solutions to Equation 26 arise for the special case where the ellipticity is zero-valued. In any material or structure this case is difficult to ensure and thus the OAM states are, in engineering practice, fragile. Hermite-Gaussian solutions arise for infinite ellipticity. For ellipticities between zero and infinity the relevant photon states are best described by Ince-Gaussians. We note that these different classifications are equivalent to selecting a coordinate system from among the choices of cylindrical, elliptical cylindrical, or rectangular, respectively.

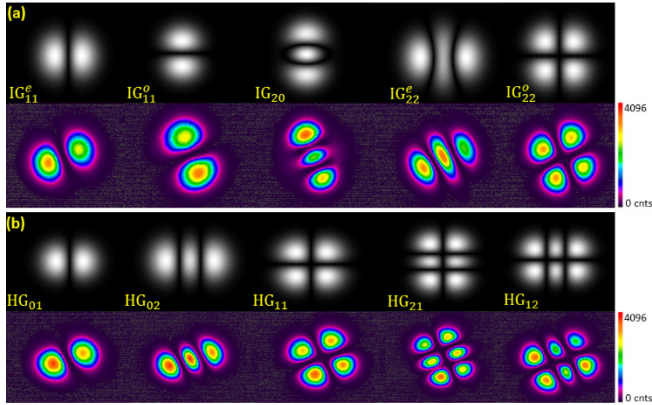


FIGURE 10

a) Comparison of Generated/Measured Hermite-Gaussian Modes (black and white) with Theoretical Computations (color); b) Comparison of Generated/Measured Ince-Gaussian Modes (black and white) with Theoretical Computations (color).

Many optical fibers and PIC processes provide waveguides that are best described by elliptical cylindrical coordinate systems, and hence our research has included detailed theoretical and experimental study of Ince-Gaussian modes [53]. Thus Ince-Gaussian states are demonstrably robust in integrated waveguide architectures and may be preferred as a photon quantum state expansion modality for higher radix spatial mode QI processing.

The use of OAM states to encode information in QPIC implementations is still largely a research endeavor and future results are forthcoming and will dictate the utility and popularity of this form of higher dimensional information encoding for QI applications. Figure 10 shows several recent experimental results obtained by generating both Hermite-Gaussian and Ince-Gaussian modes and measuring them as they exit a 100m elliptical core. These measurements are in the form of black and white images captured with a ‘charge-coupled device’ (CCD) camera. Theoretical Hermite-Gaussian and Ince-Gaussian modes are computed using MATLAB as shown in the color images in Figure 10 and compared to the experimental results indicating good agreement among the experimental measurements and theoretically predicted results.

7 SUMMARY AND CONCLUSIONS

Five decades ago, as electronic integrated circuits were rapidly scaling and maturing, there was considerable research activity involving the investigation of an appropriate radix for representing information in electronic switching

circuits including the pioneering work by Professor K.C. Smith. The classical physical characteristics of electrical charge, current and voltage were all considered as candidates for information representation; however, due to the macroscopic nature of these physical quantities, discretization required that ranges be defined and assigned to digits within a chosen corresponding fixed-radix finite number system.

As it is observed that a large majority of information processing electronic switching circuits at the time of this writing are based on binary encodings and number systems, it would appear that, in most cases, an $N = 2$ radix is considered to be the best choice, likely due to the fact that increased scaling of the total number of transistors per device due to electronic device miniaturization necessarily requires that the discretization ranges proportionately decrease in scale thus causing precision and noise margin issues to require limiting the radix to the binary case.

Here, we contrast this important topic in classical electronic switching circuit design and multiple-valued logic with the emerging, but highly analogous, topic of choosing the appropriate photonic wave function observable and a corresponding vector space dimension, N , in the design and fabrication of QPICs designed quantum informatics applications. Unlike the earlier case of electronic circuitry, QPICs do not require the specification of ranges of macroscopic physical quantities or a discretization process to convert a continuous physical measurement into a discrete set of values that encode information since there are a variety of different quantum observables associated with photonic wave functions that are already physically discrete and are thus viable candidates for representing information. Additionally, QPICs offer the possibility to exploit the quantum advantage in terms of information processing and are currently the only practical means for implementing QI processing applications at room temperature.

While no single photonic wave function conjugate variable has emerged as the best or dominant approach for QI applications, some of the most popular observables are discussed here including, polarization, location, frequency and spatial angular momentum terms. The quantum nature of these variables is surveyed with respect to their fundamental QM principles to allow this paper to be accessible to the MVL community who are familiar with the consideration of using macroscopic electrical quantities for information representation. An overview of recent results in using single photon wave function conjugate variables to represent information is provided in the hope that more readers interested in multiple-valued logic can engage and contribute further research and development in the emerging field of QPIC design. Finally, we emphasize that the important topic of information representation in integrated circuitry, as initially described by Professor K.C. Smith continues to remain very important and is a testament to his legacy.

ACKNOWLEDGEMENT

The authors thank Aviraj Sinha for proofreading this article and for converting the MS Word version into the \LaTeX format.

REFERENCES

- [1] K.C. Smith. (1976). Circuits for multiple valued logic – a tutorial and appreciation. In *Proc. Int. Symp. on Multiple-Valued Logic*, pages 30–43.
- [2] K.C. Smith. (April 1988). Multiple-valued logic: A tutorial and appreciation. *IEEE Computer Magazine*, pages 17–27.
- [3] K.C. Smith. (September 1981). The prospects for multivalued logic: A technology and applications view. *IEEE Trans. On Comp.*, C-30(9):619–634.
- [4] A.W. Elshaari, W. Pernice, K. Srinivasan, O. Benson, and V. Zwiller. (May 2020). Hybrid integrated quantum photonic circuits. *Nature Photonics*, 14:285–298.
- [5] E. Pelucchi and et al. (March 2022). The potential and global outlook of integrated photonics for quantum technologies. *Nature Reviews*, 4:194–208.
- [6] J. Wang, F. Sciarrino, A. Laing, and M.G. Thompson. (May 2020). Integrated photonic quantum technologies. *Nature Photonics*, 14:273–284.
- [7] A.F. Kracklauer. (2004). A translation of: ‘recherches sur la thorie des quanta.’. Technical report, Ann. De Phys. 10th series, t. III Janvier-Fvrier 1925.
- [8] A. Einstein. (1905). ber einen die Erzeugung und Verwandlung des liches betreffenden heuristischen Gesichtspunkt. *Annal. Physik*, 17:132–148.
- [9] R. Manenti and M. Motta. (2023). *Quantum Information Science*. Oxford University Press.
- [10] S. Slussarenko and G.J. Pryde. (October 2019). Photonic quantum information processing: A concise review. *Appl. Phys. Rev.*, 6(041303):19.
- [11] F. Flamini, N. Spagnolo, and F. Sciarrino. (2019). Photonic quantum information processing: A review. *Reports on Progress in Physics*, 82(016001):32.
- [12] M. Fox. (2006). *Quantum Optics An Introduction*. Oxford University Press.
- [13] P. Lambropoulos and D. Petrosyan. (2007). *Fundamentals of Quantum Optics and Quantum Information*. Springer.
- [14] P. Kok and B.W. Lovett. (2010). *Introduction to Optical Quantum Information Processing*. Cambridge University Press.
- [15] D.J. Griffiths and D.F. Schroeter. (2018). *Introduction to Quantum Mechanics*. Cambridge University Press, 3rd edition.
- [16] W. Heisenberg. (1927). ber den anschaulichen inhalt der quantentheoretischen kinematik und mechanik. *Zeitschrift fr Physik*, 43(3-4):172–198.
- [17] National Aeronautics and Space Administration (NASA). (1983). The actual content of quantum theoretical kinematics and mechanics. Technical Report TM-77379, NASA Technical Memorandum. (last accessed 07 September 2024).
- [18] Y.-H. Kim, S.P. Kulik, and Y. Shih. (2001). Quantum teleportation of a polarization state with a complete Bell state measurement. *Physical Review Letters*, 86(7):1370–1373.
- [19] P. Walther, K.J. Resch, T. Rudolph, E. Schenck, H. Weinfurter, V. Vedral, M. Aspelmeyer, and A. Zeilinger. (March 2005). Experimental one-way quantum computing. *Nature*, 434(7030):169–176.

- [20] J.T. Barreiro, T.-C. Wei, and P.G. Kwiat. (2010). Remote preparation of single-photon 'hybrid' entangled and vector-polarization states. *Phys. Rev. Lett.*, 105(030407).
- [21] J.J. Thorn, M.S. Neel, V.W. Donato, G.S. Bergreen, R.E. Davies, and M. Beck. (2004). Observing the quantum behavior of light in an undergraduate laboratory. *American Journal of Physics*, 72(9):1210–1219.
- [22] T.-Y. Chen, J. Zhang, J.-C. Boileau, X.-M. Jin, B. Yang, Q. Zhang, T. Yang, R. Laflamme, and J.-W. Pan. (2006). Experimental quantum communication without a shared reference frame. *Phys. Rev. Lett.*, 96(150504).
- [23] D. Bhatti, J. von Zanthier, and G.S. Agarwal. (2015). Entanglement of polarization and orbital angular momentum. *Phys. Rev. A*, 91(062303).
- [24] D.L. MacFarlane, A. Helmy, H. Shahoei, T. LaFave Jr., M.A. Thornton, E. Stewart, and W. Oxford. (2024). Towards the on-chip realization of polarization encoded QuBits. In *SPIE Int. Soc. Opt. Eng.*, volume 13028.
- [25] J.J. Sylvester. (1867). Thoughts on inverse orthogonal matrices, simultaneous sign-successions, and tessellated pavements in two or more colours, with applications to Newton's rule, ornamental tile work, and the theory of numbers. *The London, Edinburgh, and Dublin Philosophical Magazine and Journal of Science*, 34(232):461–475.
- [26] I. Bengtsson, W. Bruzda, . Ericsson, J.-. Larsson, W. Tadej, and K. yczkowski. (2007). Mutually unbiased bases and hadamard matrices of order six. *Journal of Mathematical Physics*, 48(5).
- [27] K.N. Smith and M.A. Thornton. (October 2019). Higher dimension quantum entanglement generators. *ACM Journal on Emerging Technologies in Computing Systems*, 16(1):21.
- [28] K.N. Smith, Jr. T.P. LaFave, D.L. MacFarlane, and M.A. Thornton. (2019). A radix-4 Chrestenson gate for optical quantum computation. *Journal of Applied Logics*, 5(9):1781–1798.
- [29] A. Sinha, E.R. Henderson, J.M. Henderson, and M.A. Thornton. (November 2022). Automated quantum memory compilation with improved dynamic range. In *Proc. Int. Workshop on Quantum Computing Software (QSC22, part of Int. Conf. for High Performance Computing, Networking, Storage, and Analysis, SC22)*, page 14.
- [30] M.A. (Mitchell) Thornton, W.V. Oxford D.L. MacFarlane, and M.A. (Micah) Thornton, (2024). Systems and methods for multi-source true random number generators. U.S. Patent 11,989,532.
- [31] L. Olislager, J. Cussey, A.T. Nguyen, Ph. Emplit, A. Massar, J.-M. Merolla, and P. Huy. (2010). Frequency bin entangled photons. *Physical Review A*, 82(1):013804.
- [32] M. Cabrejo-Ponce, A.L.M. Muniz, M. Huber, and F. Steinlechner. (2023). High-dimensional entanglement for quantum communication in the frequency domain. *Lasers and Photonics Reviews*, 17.
- [33] P. Treutlein. (November 2016). Photon qubit is made of two colors. *Physics*, 9.
- [34] W. Bogaerts and et al. (2012). Silicon microring resonators. *Laser Photonics*, 6(1):47–73.
- [35] Y.R. Bawankar and A. Singh. (2021). Microring resonators based applications in silicon photonics – a review. In *Proc. IEEE Conf. on Information and Communication Technology (CICT)*.
- [36] A. Mirza and et al. (October 2022). Silicon photonic microring resonators: A comprehensive design-space exploration and optimization under fabrication-process variations. *IEEE Trans. on CAD*, 41(10):3359–3372.

- [37] M. Kues et al. (June 2017). On chip generation of high-dimensional entangled states and their coherent control. *Nature*, 546(7660):622–626.
- [38] J.M. Lukens and P. Lougovski. (January 2017). Frequency-encoded photonic qubits for scalable information processing. *Optica*, 4(1):8–16.
- [39] I. Chuprina and A.A. Kalachev. (October 2019). Generating frequency-bin qubits via spontaneous four-wave mixing in a photonic molecule. *Physical Review A*, 100(4):043843.
- [40] H.-H. Lu, A.M. Weiner, and P. Lougovski. (December 2019). Quantum information processing with frequency-comb qudits. *IEEE Photonics Letters*, 31(23):1858–1861.
- [41] G.L. Li and P.K.L. Yu. (September 2003). Optical intensity modulators for digital and analog applications. *Journal of Lightwave Technology*, 21(9):2010–2030.
- [42] P. Kolchin, C. Belthangady, S. Du, G.Y. Yin, and S.E. Harris. (September 2008). Electro-optic modulation of single photons. *Physical Review Letters*, 101(10):103601.
- [43] M. Yeh. (2020). Integrated electro-optic modulators: Progress, challenges, and opportunities. Technical report, Online open source technical report. (last accessed September 10, 2024).
- [44] G. Sinatkas, T. Christopoulos, O. Tsilipakos, and E.E. Kriezis. (July 2021). Electro-optic modulation in integrated photonics. *Journal of Applied Physics*, 130:010901.
- [45] D. Hah. (2016). Design of wide-band tunable optical filters with cascaded microring resonators and shaped-finger comb-drive actuators. In *Proc. IEEE Symposium on Design, Test, Integration & Packaging of MEMS and MOEMs*, page 5.
- [46] B.E. Nussbaum, A.J. Pizzimenti, N.B. Lingaraju, H.-H. Lu, and J.M. Lukens. (2022). Design methodologies for integrated quantum frequency processors. *Journal of Lightwave Technology*, 40(23):7648–7657.
- [47] H.-H. Lu, M. Liscidini, A.L. Gaeta, A.M. Weiner, and J.M. Lukens. (December 2023). Frequency-bin photonic quantum information. *Optica*, 10(12):1655–1671.
- [48] M. Agnew, J. Leach, M. McLaren, F.S. Roux, and R.W. Boyd. (2011). Tomography of the quantum state of photons entangled in high dimensions. *Physical Review A – Atomic, Molecular, and Optical Physics*, 84:062101.
- [49] M. Mirhosseini, M. Malik, Z. Shi, and R.W. Boyd. (2013). Efficient separation of the orbital angular momentum eigenstates of light. *Nature Communications*, 4:2781.
- [50] M. Malik, M. Mirhosseini, M.P.J. Lavery, J. Leach, M.J. Padgett, and R.W. Boyd. (2014). Direct measurement of a 27-dimensional orbital-angular-momentum state vector. *Nature Communications*, 5:3115.
- [51] M. Mirhosseini, O.S. Magaña-Loaiza, M.N. O’Sullivan, B. Rodenburg, M. Malik, M.P.J. Lavery, M.J. Padgett, D.J. Gauthier, and R.W. Boyd. (2015). High-dimensional quantum cryptography with twisted light. *New Journal of Physics*, 17:033033.
- [52] F. Cardano, E. Karimi, S. Slussarenko, L. Marrucci, C. de Lisio, and E. Santamato. (2012). Polarization pattern of vector vortex beams generated by q-plates with different topological charges. *Applied Optics*, 51:C1–C6.
- [53] S. Sakpal, G. Milione, M.-J. Li, M. Nouri, H. Shahoei, T. LaFave Jr., S. Ashrafi, and D. MacFarlane. (2018). Stability of InceGaussian beams in elliptical core few-mode fibers. *Optics Letters*, 43:2656–2659.